Atmos. Chem. Phys., 6, 4067–4077, 2006
www.atmos-chem-phys.net/6/4067/2006/
© Author(s) 2006. This work is licensed
under a Creative Commons License.

Atmospheric Chemistry and Physics

A scaling analysis of ozone photochemistry

B. Ainslie and D. G. Steyn

Atmospheric Science Programme, The University of British Columbia, Vancouver, Canada

Received: 14 October 2005 – Published in Atmos. Chem. Phys. Discuss.: 19 December 2005
Revised: 3 July 2006 – Accepted: 15 August 2006 – Published: 11 September 2006

Abstract. A scaling analysis has been used to capture the integrated behaviour of several photochemical mechanisms for a wide range of precursor concentrations and a variety of environmental conditions. The Buckingham Pi method of dimensional analysis was used to express the relevant variables in terms of dimensionless groups. These grouping show maximum ozone, initial NO_x and initial VOC concentrations are made non-dimensional by the average NO_2 photolysis rate (j_{av}) and the rate constant for the NO–O_3 titration reaction (k_{NO}); temperature by the NO–O_3 activation energy (E_{NO}) and Boltzmann constant (k) and total irradiation time by the cumulative $j_{av}\Delta t$ photolysis rate. The analysis shows dimensionless maximum ozone concentration can be described by a product of powers of dimensionless initial NO_x concentration, dimensionless temperature, and a similarity curve directly dependent on the ratio of initial VOC to NO_x concentration and implicitly dependent on the cumulative NO_2 photolysis rate. When Weibull transformed, the similarity relationship shows a scaling break with dimensionless model output clustering onto two straight line segments, parameterized using four variables: two describing the slopes of the line segments and two giving the location of their intersection. A fifth parameter is used to normalize the model output. The scaling analysis, similarity curve and parameterization appear to be independent of the details of the chemical mechanism, hold for a variety of VOC species and mixtures and a wide range of temperatures and actinic fluxes.

1 Introduction

The link between NO_x, mixtures of volatile organic compounds (VOCs) and sunlight in the production of ground level ozone was first recognized in the Los Angeles area in the 1940s (Haagen-Smit, 1952). Since that time, a great deal of effort has been directed at understanding tropospheric photochemistry. This research is complicated by the large number of VOC species found in urban environments and the manifold reaction paths in which these species can participate - an explicit treatment of ozone formation would require thousands of reactants participating in an even greater number of reactions (Atkinson, 2000). To simplify the representation of these reactions in computer models, different means of condensing the chemistry have been employed, typically yielding chemical mechanisms with 30 to 50 species and between 80 and 200 reactions (Dodge, 2000). While this represents a significant reduction, the resulting mechanisms remain complex.

It is not surprising, then, that various highly idealized models, aimed at encapsulating the most important photochemical processes in as compact form as possible, have been developed alongside these chemical mechanisms. For example Johnson (1984) has developed an analytical model for ozone photochemistry, using smog chamber data, to express the relationship between primary smog products (amount of ozone produced and NO converted to NO_2) and initial VOC and NO_x concentrations, in terms of simple formulae. The relationships are valid over a wider range of precursor conditions but appear to provide an incorrect sensitivity to initial NO_x concentration (Blanchard et al., 1999). Statistical and regression techniques have also been used to capture the behaviour of chemical systems: Shenvi et al. (2004) use a neural network to represent the behaviour of an explicit formaldehyde oxidation scheme in terms of a limited number of input variables; Wang et al. (2001) map the output of box model simulations onto a small set of input variables, using an expansion of correlated functions, to develop a high dimensional model representation of a chemical mechanism; Chang and Rudy (1993) develop a relationship for the ozone response surface of a photochemical mechanism in

Correspondence to: B. Ainslie
(bainslie@eos.ubc.ca)

Published by Copernicus GmbH on behalf of the European Geosciences Union.

terms of initial VOC, NO_x concentrations and temperature, through a non-linear function minimization routine. A third approach to understanding the behaviour of a complex system is through the use of a simplified physical system: Azzi et al. (1992) develop a highly parameterized set of chemical reactions, involving only a few species, to provide a conceptual framework for ozone photochemistry, though their "mechanism" appears to incorrectly model ozone formation in the low VOC/NO_x regimes (Tonnesen and Jeffries, 1994).

The aim of this paper is to use a scaling-level analysis as a means of developing a simple model for the behaviour of a photochemical mechanisms. This type of analysis, which looks for similarities between systems or phenomena which are actually different, has been applied to a wide range of complex systems including: physical (Taylor, 1950), biological (West et al., 1997) and hydrodynamical (Birkhoff, 1950). It can be used to determine the minimum number of essential measurements in experimental work, provide an effective way of displaying large data sets, or reduce complex systems to a simpler form (Bridgman, 1937, Barenblatt, 1996). While the aim of this analysis is to capture essence of ozone photochemistry while excluding a great many details, we are not implying these details are unimportant, but, rather that their influence is often overshadowed by more dominant processes or can be accounted for by using carefully selected variables.

2 Scaling analysis

While photochemical mechanisms consist of hundreds of competing reactions having a variety of timescales, qualitatively they can be understood in terms of an interconnected NO_x and radical cycle, each driven by sunlight (Jeffries and Tonnesen, 1994). The first cycle involves the photolysis of NO_2 and titration of O_3 by NO and consists of relatively fast inorganic reactions. The second cycle involves the slow conversion of NO-to-NO_2 via organic peroxy radicals produced in catalytic chain reactions initiated by $OH^\bullet$ attack on VOCs. It is the integrated effect of these organic reactions that leads to high ozone concentrations seen in and around many polluted urban environments. Guided by this conceptual model, we use the Buckingham Pi method of scaling analysis – a systematic approach to dimensional analysis in which all relevant physical variables are placed into dimensionless groups (Stull, 1988) – to express the integrated behaviour of a photochemical mechanism in terms of a small set of non-dimensional groups.

Thus, in a hypothetical box of air having volume V, we expect the maximum amount of ozone (N_{O_3}) produced from an initial amount of VOC (N_{VOC}) and NO_x (N_{NO_x}), will be a function of: the average NO_2 photolysis rate constant (j_{av}), the length of time the mixture is irradiated (Δt), the activation energy (E_{NO}) and molecular collision rate (A_{NO}) for the NO–O_3 titration rate. Because $OH^\bullet$ attack represents a rate limiting step in ozone formation, we use the activation energy of the VOC–$OH^\bullet$ reaction (E_{OH}), it's collision rate (A_{OH}) and the average molecular translational energy (kT) as measures of the importance of the organic reactions.

We have identified eleven different variables having four separate fundamental dimensions of length, time, mass and amount of substance (Table 1 summarizes the relevant variables and their dimensions). Dimensional analysis allows us to select any four of these variables (equal to the number of fundamental dimensions) to non-dimensionalize the remaining variables provided all of the fundamental dimensions are represented by the key variables and the key variables cannot be arranged into a single non-dimensional group. We choose kT, V, j_{av} and A_{NO} to non-dimensionalize the remaining variables giving the following seven (11 variables – 4 fundamental dimensions) dimensionless groups:

$$\pi = \frac{N_{O_3} A_{NO}}{V j_{av}},\ \pi_1' = \frac{N_{VOC} A_{NO}}{V j_{av}},\ \pi_2 = \frac{N_{NO_x} A_{NO}}{V j_{av}} \qquad (1)$$
$$\pi_3 = j_{av}\Delta t,\ \pi_4' = \frac{E_{OH}}{kT},\ \pi_5' = \frac{E_{NO}}{kT},\ \pi_6 = \frac{A_{NO}}{A_{OH}}$$

Next, to assist in the analysis and without loss of generality, we form new dimensionless groups from these seven. A new π_1 is formed by dividing π_1' by π_2 and represents the initial relative abundance of VOC to NO_x. Next, since molecular collision theory shows the partitioning of molecules with energy sufficient for bond breaking has an exponential dependence on both the activation and translational energy, π_4' and π_5' are rewritten using exponentials, $\pi_4 = \exp\{\pi_4'\}$ and $\pi_5 = \exp\{\pi_5'\}$.

The premise of dimensional analysis is that given a complete set of independent variables that account for the behaviour of a system, then a subset of dimensionally independent variables can be found which also captures the system behaviour. Thus, assuming the original dimensional variables account for all of the important processes, then dimensional analysis suggests the relationship between maximum ozone and its governing variables can be expressed by:

$$\pi = \hat{f}(\pi_1, \pi_2, \pi_3, \pi_4, \pi_5, \pi_6) \qquad (2)$$

where $\hat{f}$ is an unknown function of only six independent (dimensionless) variables. While this marks the end of the formal Buckingham Pi analysis, we make three further simplifications.

First, for Arrhenius type reactions, A_{NO} and A_{OH} are independent of temperature, their ratio becomes a constant and so π_6 will not influence the functional form of the similarity relationship and can be ignored.

Second, we observe for an O_3-NO-NO_2 system (i.e. one without VOCs), steady state ozone concentration scales with j/k_{NO}:

$$\frac{[O_3]_{ss}}{j/k_{NO}} = \frac{[NO_2]_{ss}}{[NO]_{ss}} \qquad (3)$$

Table 1. Physical quantities which affect ozone concentrations in a hypothetical box of air with their *SI* units and dimensions.

Variable	Description	Units	Dimensions
V	Volume	m^3	$length^3$
N_{O_3}	Maximum amount of ozone	moles	number
N_{NO_x}	Initial amount of NO_x	moles	number
j_{av}	Average NO_2 photolysis rate constant	sec^{-1}	$time^{-1}$
A_{NO}	NO-O_3 collision frequency	$cm^3(molecules \cdot s)^{-1}$	$length^3(number \cdot time)^{-1}$
E_{NO}	Activation energy for O_3+NO titration	$J\,molecule^{-1}$	$mass \cdot length^2 \cdot time^{-2} \cdot number^{-1}$
N_{VOC}	Initial amount of VOC	moles	number
Δt	Length of test	sec	time
A_{OH}	VOC-OH collision frequency	$cm^3(molecules \cdot s)^{-1}$	$length^3(number \cdot time)^{-1}$
E_{OH}	Activation energy for VOC+$OH^{\cdot}$ reaction	$J\,molecule^{-1}$	$mass \cdot length^2 \cdot time^{-2} \cdot number^{-1}$
kT	Average molecular translational energy	$J\,molecule^{-1}$	$mass \cdot length^2 \cdot time^{-2} \cdot number^{-1}$

For our O_3-NO_x-VOC system, a similar scaling for ozone can be achieved by dividing π by π_5:

$$\pi/\pi_5 = \frac{N_{O_3}}{\frac{V \cdot j_{av}}{A_{NO} \exp[-E_{NO}/(kT)]}} = \frac{[O_3]_{max}}{j_{av}/k_{NO}} \quad (4)$$

where $[O_3]_{max}$ ($=N_{O_3}/V$) is the maximum ozone concentration and
k_{NO} ($=A_{NO} \exp\{-E_{NO}/kT\}$) the Arrhenius rate constant for the NO-ozone titration reaction. Accordingly, we scale the dimensionless number of moles of NO_x (π_2) by π_5 and guess the functional dependence of π_5 can be approximated via π/π_5 and π_2/π_5.

Third, we try a power law for the π_2/π_5 dependence on π/π_5. This last assumption is guided by the work of Chang and Rudy (1993), Blanchard et al. (1999), and Johnson (1984) who all suggest that maximum ozone concentration scales with a power of initial NO_x concentration. To assist in the analysis, in Table 2 we list the main non-dimensional groups, express them in terms of their dimensional quantities and, based on the underlying physical quantities, introduce for each a new symbolic name.

The objective is then to search for empirical relations of the form:

$$\frac{\pi}{\pi_5} = \left(\frac{\pi_2}{\pi_5}\right)^a f(\pi_1, \pi_3, \pi_4) \quad (5)$$

or equivalently

$$\overline{[O_3]} = \overline{[NOx]}^a \; f(R, J, \overline{T}) \quad (6)$$

where a is an unknown exponent and the unknown function (f) is now only dependent on three dimensionless groups.

To start, we use the RADM2 photochemical mechanism (Stockwell et al., 1990) to simulate the photochemical oxidation of the RADM2 propene surrogate (OLT) at constant temperature and for a time varying actinic flux consistent with a single location and date. We use the model output to find the functional form of $f(R)$. Then we examine simulations using different VOCs and VOC mixtures. The analysis is then extended to include a range of temperatures ($\overline{T}$) and different total actinic fluxes (J).

2.1 OZIPR simulations

To generate model output, a matrix of 121 simulations using the OZIPR (Tonnesen, 2000) trajectory model was run using the RADM2 chemical mechanism. In order to facilitate the interpretation of our results, we study the photochemistry in isolation from both mechanical and environmental processes i.e. we simulate a well mixed parcel of air free from dilution, entrainment, deposition or "wall-effects"; which is kept at a constant temperature of 25°C; and exposed to a total dimensionless actinic flux of J=347 (corresponding to Vancouver B.C. in mid-summer (3 August) with simulation start time at 07:00 a.m. (local solar time (LST)) and end time at 06:00 p.m. LST). We create the test matrix by independently varying the initial OLT and NO_x concentrations in 10% increments within a 0.0 and 0.6 ppm OLT range and a was 0.0 to 0.15 ppm NO_x range. The simulations produced an overall maximum modeled ozone concentration of 348 ppb.

Model output consisted of maximum ozone concentration along with initial OLT and NO_x concentrations. However, before the model output was analyzed, some simulations were excluded. Whenever initial NO_x concentration was zero (and R infinite), the RADM2 mechanism produced no ozone and these trivial simulations were removed. In addition, whenever initial OLT concentration were zero (R=0), the RADM2 mechanism produced low ozone concentrations, independent of OLT, representing ozone formation in a NO_x-only system. Since the scaling analysis is concerned with VOC–NO_x systems, these simulations were also excluded. After these removals, 100 simulations remained to determine $f(R)$.

Table 2. List of pi-groups, their dimensional quantities and new symbolic names.

Pi-group	Dimensional Quantities	Description	Symbolic name
π/π_5	$\frac{[O_3]_{max}}{j_{av}/k_{NO}}$	Non-dimensional ozone	$\overline{[O_3]}$
π_2/π_5	$\frac{[NOx]_o}{j_{av}/k_{NO}}$	Non-dimensional NO_x	$\overline{[NOx]}$
π_1	$[VOC]_o/[NOx]_o$	Initial precursor concentration ratio	R
π_3	$j_{av}\Delta t$	Non-dimensional actinic flux	J
π_4	$\exp\{E_{OH}/kT\}$	Non-dimensional temperature	$\overline{T}$

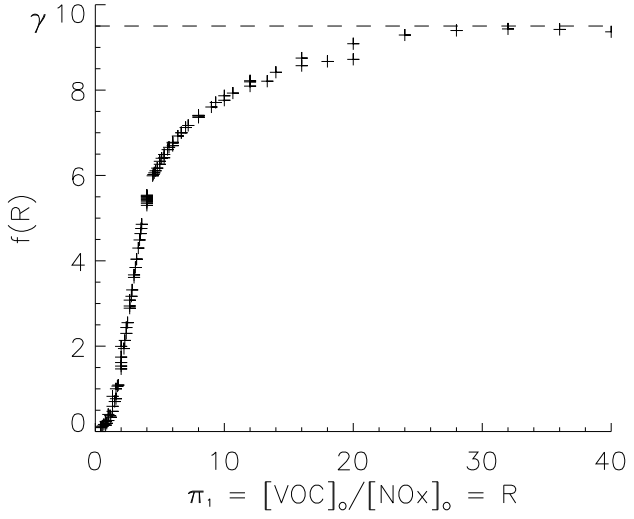

Fig. 1. Dimensionless ozone scaled by dimensionless initial $NO_x{}^a$ versus ratio of initial precursor concentration (R). Model output from RADM2 (Stockwell et al., 1990) simulations using OLT as the sole VOC, a constant temperature of 25°C and a total dimensionless actinic flux of J=347. Dashed line shows limiting value (γ) for the similarity relationship.

2.2 Similarity relationship

Using Eq. (5), modeled maximum ozone concentration was made dimensionless and scaled by a power of dimensionless initial NO_x i.e.:

$$\frac{[O_3]_{max}}{j_{av}/k_{NO}} \Big/ \left(\frac{[NO_x]_o}{j_{av}/k_{NO}}\right)^a = f(R) \tag{7}$$

It was found that with a value of a=0.6, model output, when plotted using Eq. (7), and as a function of R, collapsed onto a single common curve (Fig. 1); suggesting success in the scaling analysis. It must be pointed out that this curve does not plot the time evolution of ozone for a single simulation, but rather, it shows scaled maximum ozone concentration (from many different simulations) divided by scaled initial NO_x concentration (raised to a power a) versus initial VOC to NO_x concentration from the various simulations.

This curve shows a sigmoid shape (the small hook at low R-values has been compressed in this plot because of the need to plot a large range of R-values) hints at a parameterization using a Weibull function. The idea for such parameterization is guided by Chang and Rudy (1993) who using model output, found the function:

$$\phi(R) = 1 - \exp\left\{-aR^b\right\} \tag{8}$$

fit their NO_x-scaled, dimensional ozone concentrations well. This expression, chosen because of its simple functional form (Chang and Rudy, 1993), can be expressed as a Weibull function after the transformation b=α and a=$\beta^{-\alpha}$.

To test the suitability of the Weibull function, the dimensionless model output was normalized and transformed using the inverse Weibull function:

$$W(f(R)) = \ln\left(\ln\left(\frac{1}{1 - f(R)/\gamma}\right)\right) \tag{9}$$

If the Weibull function fits the similarity relationship, then the transformed model output should cluster along a straight line when plotted as a function of ln R (Fig. 2).

From this figure, it is evident that the dimensionless model output collapses not onto one, but two straight lines, which separates the similarity relationship into two regions characterized by a change in slope at ln R≈1.3 (R≈3.7). This shift hints at a change in governing chemical process; perhaps evidence of the change in ozone sensitivity to changing NO_x concentration across the ridgeline.

The dashed line the Fig. 2 defines two regions: Region I, to the right of the break and regions II to the left. Within each of these regions dotted lines indicate ln R-values where more scatter appears. The scatter for low ln R values, associated with simulations having low OLT/high NO_x concentrations, stems from a slight dependence of the NO_x-scaling exponent (a) on R. The increased scatter and slight hook in the model output at high ln(R) is explored in Sect. 3.2.

A parameterization for the similarity relationship, which captures the scaling break, has been developed. It is a composite of two Weibull functions with shape parameter (α) that varies as a function of R:

$$f(R)/\gamma = 1 - \exp\left\{-\lambda\,(R/\beta)^{\alpha(R)}\right\} \tag{10}$$

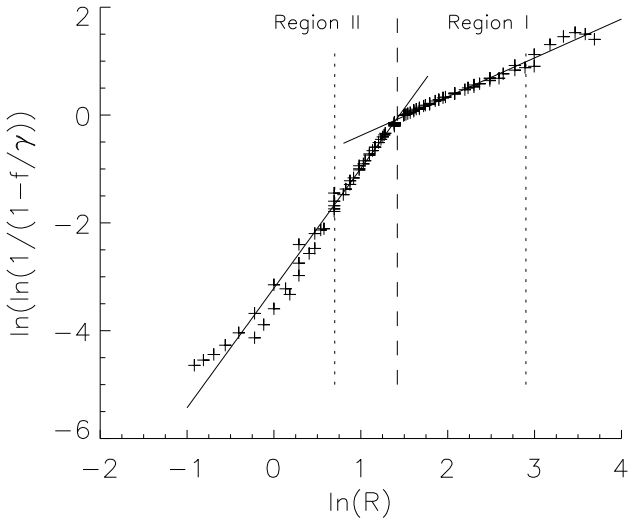

Fig. 2. Scaled model output after the Weibull transformation. To highlight the clustering of model output onto two line segments, a pair of solid lines has been included. Also shown are three vertical lines separating the plot into four regions. The dashed line at ln R=1.3 marks the change in slope while the two dotted lines mark the regions of increased scatter.

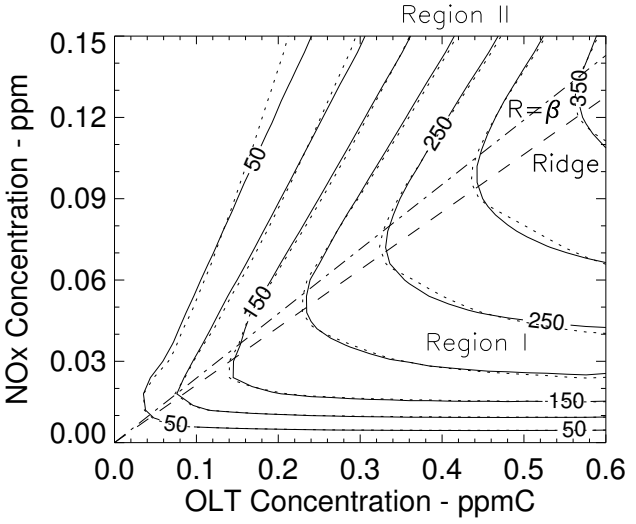

Fig. 3. Ozone isopleth (in ppb) for the NO_x-OLT system. Solid lines are isopleths from OZIPR model. Dotted isopleths are based on the similarity function. Also shown is the ridgeline (dashed line labeled Ridge), scaling break (dot-dashed line labeled R=β) and Regions I and II.

$$\alpha(R) = \begin{cases} \alpha_1, & R < \beta \\ \alpha_2, & R \geq \beta \end{cases}$$

When α_1=α_2 and λ=1, a Weibull function is recovered. When $R \to \infty$ (the relative abundance of VOC to NO_x is large) $f(R) \to \gamma$ and maximum ozone concentration is a function of initial NO_x concentration only (which we call the NO_x-only scaling (NOS) regime) consistent with Chang and Suzio (1995), Blanchard et al. (1999) and Johnson (1984). Thus we find six parameters are needed to parameterize the OLT chemistry: one to normalize the scaled model output (γ), one for the NO_x scaling exponent (a), two for the location of the scaling break (β,λ) and two for the slopes of the line segments (α_1,α_2) (in the Weibull plane).

We use Eqs. (10) and (5) to plot predicted and modeled maximum ozone isopleths in Fig. 3. A line of constant R, associated with the scaling break (β), has also been plotted. The ridgeline, as determined by the location where the sensitivity of ozone to changing NO_x concentrations is zero has also been drawn. It has a value of $R \approx 4.8$, and appears to lie below the scaling break. From Figure 3, we see that the similarity relationship fits the ozone isopleths quite well in most of the domain but with the similarity function diverging from the model output at the lowest $[OLT]_o/[NO_x]_o$ values.

3 Other VOC classes and VOC mixtures

Analyses have been carried out for all RADM2 classes in addition to several VOC mixtures. A selection of the resulting Weibull transformed similarity relationships is given in Fig. 4, and, with the exception of low reactive ethane surrogate (ETH) in Fig. 4a) and the pentane-like alkanes (H5C) with moderate $OH^\bullet$ reactivities in Fig. 4b, all similarity relationships show model output clustering onto two distinct line segments separated by a scaling break. In order to capture the wide range of oxidation behaviours exhibited by the RADM2 classes, initial NO_x and VOC concentrations, as well as test matrix size, were adjusted for each set of simulations. In general, initial NO_x concentrations were chosen so that greatest maximum ozone concentration (peak concentration) was between 100 and 300 ppb – a range considered representative of elevated but not unrealistically high ozone pollution concentrations (National Research Council, 1991). Next, initial VOC concentrations were chosen so that there was roughly an equal number of simulations in on either side of the scaling break (β). Finally, the number of simulations was chosen so that the similarity relationship ($f(R)$) exhibited asymptotic behaviour for large R-values. This final constraint required adjusting the increment size for the test matrix; smaller increments giving rise to more simulations over a wider range of R-values. For this work only two increments sizes where used: 10% and 2.5% giving 121 and 1681 simulations respectively. This last constraint introduces a difficulty with the analysis: in order to capture the asymptotic behaviour of the similarity relationship, and in order to keep an equal number of simulations on either side of the scaling break, some VOCs were analyzed over a greater range of precursor conditions than others. However, we find the scaling behaviour holds only over a finite range of precursor

concentrations (Ainslie, 2004). Thus, the photochemistry of some VOCs, over the chosen range of conditions that covers the VOC- and NO_x-limited regions as well as the ridgeline, is easier to parameterize than others and comparisons of results must take this range into account.

3.1 Alkane classes (ETH, HC3, HC5 and HC8) and non-reactive class (NR)

In general, unreactive VOCs (principally the alkanes) were the most difficult to scale and were poorly fit by the similarity relationship. The ethane surrogate ETH (Fig. 4a) produces a break around $R \approx 670$ but requires R-values greater than 22000 to reach its asymptotic value. Furthermore, the NO_x-scaling exponent (a) shows an R-dependence which leads to increased scatter over the large range of R-values shown. The alkane class with the next lowest $OH^{\bullet}$-reactivities (HC3) produced similar trends (not shown). Surprisingly, the higher alkane classes HC5 (Fig. 4b) and HC8 (not shown) showed poorer scaling than the ethane and HC3 class. The non-reactive class did not appear to scale with any power of $[NO_x]^a$ (not shown).

It is likely in the alkane simulations, with the low $OH^{\bullet}$-reactivities and limited organic radical sources, the conceptual model used to identify key variables is incomplete. For example, the poor scaling shown by the HC8 class likely arises from increased NO_x and peroxy radical losses due to increased organic nitrate formation – reaction pathways whose effects would require the inclusion of new dimensionless groups into the scaling analysis.

3.2 Alkene classes (OL2, OLI and OLT)

Of the three alkene classes, the ethene class (OL2) was the hardest to fit, likely due to its low $OH^{\bullet}$-reactivity and produced results similar to ETH but with less scatter at low $\ln(R)$ (not shown). OLI (the surrogate for alkenes with internal double bonds) showed good scaling and, like OLT, shows a distinct second break in the Weibull transformed model output at high R-values (Fig. 4c). This marks the beginning of a new scaling regime where alkene+O_3 reactions are important. This new trend, difficult to see on an isopleth diagram because these diagrams compress the response surface along the VOC-axis for high R-values, is not of immediate concern since this regime is greatly removed from the ridgeline where parameterizing the photochemistry is of greatest interest.

3.3 Aromatics (TOLU and XYLE)

Results for the aromatic classes TOLU, representative of toluene and less reactive organics is given in Fig. 4d. It, and the XYLE aromatic class (representing xylenes and more reactive aromatics (not shown)), show more scatter than alkenes but still produce a break in the Weibull transformed model output and are well parameterized by the similarity function.

3.4 Carbonyl (HCHO, ALD and KET)

RADM2 explicitly models formaldehyde and this class (HCHO) proved difficult to scale due the extremely large R-values required to capture it's asymptotic behaviour and the modest kink in the Weibull transformed model output (Fig. 4e). The slight break, caused by the shallow slope in the low $\ln(R)$ line segment, stems from the photolysis of formaldehyde acting as a strong organic radical source and is further discussed in a companion paper. The large range of R-values required to reach an asymptotic value appears to be related to its inability to produce PAN or ONIT precursors; requiring all NO_x to be converted to HNO_3 before photochemical production ceases (Ainslie, 2004). The higher aldehyde class (ALD) proved to be the best class to model with good agreement between the similarity function and model output everywhere except at the very lowest R-values (Fig. 4f). The ketone class (KET) was also well modeled (not shown).

3.5 Mixtures

Two VOC mixtures, representative of polluted urban environments, were also modeled using RADM2. The first mixture was an Air Resources Board (ARB) modified version of the (Jeffries et al., 1986) analysis of the Lonneman (Lonneman, 1986) 29 city VOC canister study (Fig. 4G). The second was a mixture used by Stockwell et al. (1997) for his comparison of his RADM2 model and the Regional Atmospheric Chemistry Mechanism (RACM) model (not shown). Both mixtures show good scaling with a distinct scaling break and slight deviations at very low R-values.

3.6 Other mechanisms

To test whether the scaling is a particularity of the RADM2 mechanism, three additional chemical mechanisms were examined: CB-IV (Gery et al., 1989), SAPRC (Carter, 1990) and the master chemical mechanism (MCM) (Saunders et al., 1997). The first two mechanisms use entirely different approaches to condensing the photochemistry than RADM2 while the third provides a near explicit description of the gas phase tropospheric oxidation of over 120 VOC compounds. Any scaling of $[O_3]_{max}$ observed from these mechanism strengthens the premise that complex photochemical processes can be described using a small set of variables – at least to the extent that numerical models capture the chemical processes. While only the CB-IV and MCM results are discussed here, the SAPRC model produced results similar to the RADM2 mechanism.

Two simulations were run using CB-IV. The first, using CB-IV classes PAR and OLE to represent propene, showed good scaling and produced a scaling break (not shown). The second (Fig. 4h) simulated the ARB urban mixture used in the RADM2 simulations and produced a similarity

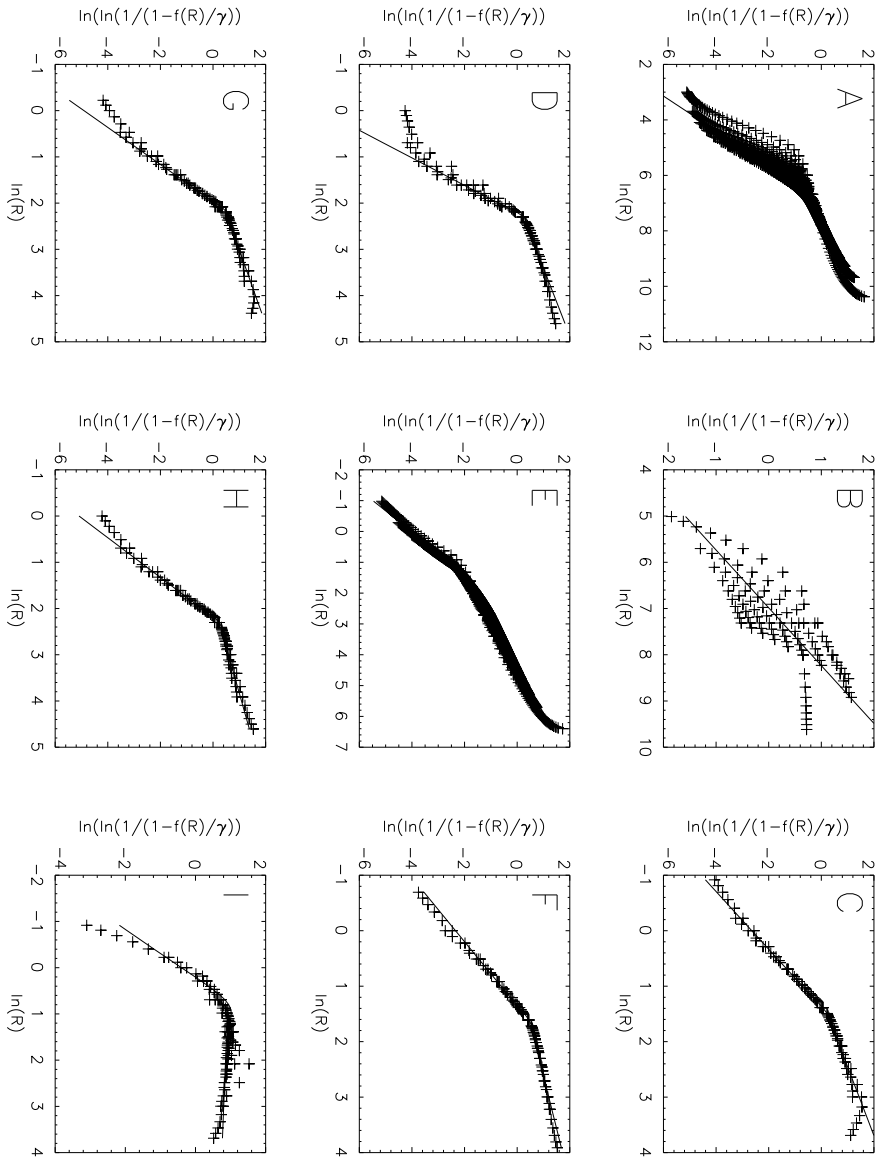

Fig. 4. Weibull transformed similarity relationships for RADM2 classes: A) ETH B) HC5 C)TOLU D) OLI E) HCHO F) ALD. An urban VOC mixture is simulated using G) the RADM2 mechanism and H)CB-IV mechanism. Finally, results from MCM using propene are given in I). In each plot model output is given by "+" signs and the similarity function by solid lines.

relationship almost identical to the RADM2 ARB mixture (Fig. 4g). The MCM propene results, given in Fig. 4i, show a less distinct break than the RADM2 OLT results (Fig. 2) with the MCM similarity relationship showing a slight downward trend for $\ln(R)>1$, suggesting enhanced ozonolysis in the MCM mechanism. There is also more scatter in the similarity relationship especially near $\ln(R)=3$ and $\ln(R)=4$.

4 Variability of scaling parameters with J and $\overline{T}$

To examine the combined effects of varying actinic flux (J), temperature ($\overline{T}$) and initial precursor concentration (R and $\overline{[\mathrm{NOx}]}$) on the scaling analysis, OZIPR simulations were performed for an OLT-NO_x-O_3 system at five different J-values (204, 228, 257, 287 and 319 corresponding to five summer dates encompassing the typical ozone season in Vancouver, B.C. (Pryor and Steyn, 1995)) and at four different temperatures (20, 25, 30 and 35°C). This gave a total of 20 scenarios with each consisting of 121 simulations of varying initial OLT and NO_x concentrations.

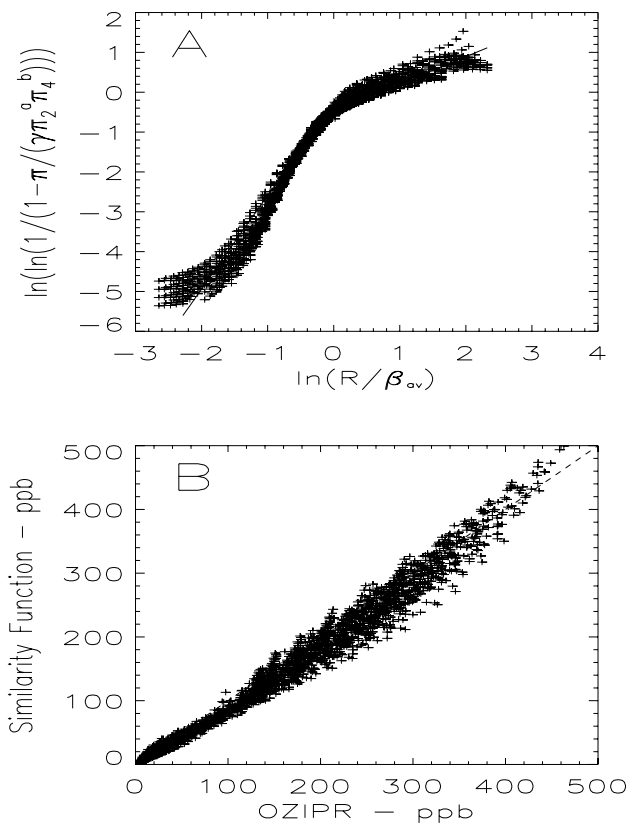

Fig. 5. Weibull transformed model output for RADM2 simulations having five different levels of actinic flux and four different temperatures after horizontal translation by $\ln \beta_{av}$ **(a)**. The corresponding scatter plot of maximum ozone concentrations as calculated by OZIPR and as predicted by the "universal" similarity function is given in **(b)**. The dashed line visible at the top of this figure is the 1:1 line.

4.1 "Universal" similarity relationship

To find a "universal" similarity relationship which includes the J and $\overline{T}$ dependencies, modeled maximum ozone and initial NO_x concentrations, from each of the 2000 (20×100) non-trivial simulations, were first made dimensionless by k_{NO} and j_{av} (dependent on simulation temperature and actinic flux respectively). Next a power law was tried for the $\overline{T}$-dependence, and dimensionless maximum ozone was scaled by $\overline{[NOx]}^a$ and $\overline{T}^b$ (found iteratively and explained below). The resulting largest value for $\overline{[O_3]}/(\overline{[NOx]}^a \overline{T}^b)$ was used as a normalizing constant (γ). The resulting model output was Weibull transformed and plotted as a function of $\ln R$ which revealed a family of separate curves, distinguished by their J-values and horizontally translated from one another. To get these curves to collapse onto a "universal" curve, each curve was translated so their scaling breaks coincided. This amounted to a translation by $\ln \beta_{av}$ where β_{av} is the average β-value for each J-level (the β-values showed a slight $\overline{T}$ dependence). The amount of translation was parameterized using a power law:

$$\beta_{av} = \beta' J^{-c} \tag{11}$$

where β' and c were found by regressing β_{av} against J.

Figure 5a shows all the 20 sets of Weibullized transformed model output after translating by $\ln \beta_{av}$. The Figure shows large scatter for both $\ln(R/\beta)<-1.0$ and $\ln(R/\beta)>1.0$. One simulation (J=204 T=20°C) appeared to deviate from the others. This simulation had the lowest J-value and lowest temperature. This low flux/low temperature simulation suggests a limit of applicability to the scaling regime and was not used in the determination of the similarity function. Also plotted in Fig. 5 is the similarity function fitted to the model output from the 19 other scenarios. Values for the scaling powers (a and b) as well as the similarity parameters (α_1,α_2,λ) were found by minimizing the RMSE between the similarity function and OZIPR model output where the function was forced to fit the model output more closely around the ridgeline area (defined by $\ln(R/\beta_{av}) \in [-1.61, 1.61]$). The corresponding scatter plot maximum ozone concentration as calculated by OZIPR and predicted by the "universal" similarity function is given in Fig. 5b. Visible in the upper right hand corner of this figure is the 1:1 line. The scatter plot shows the "universal" similarity function does an excellent job of capturing the variability of maximum ozone concentrations over a wide range of temperatures, actinic fluxes and VOC and NOx concentrations.

4.2 Universal propene curve

Based on the above analysis, the "universal" curve OLT has the form:

$$\frac{[O_3]_{\max}}{j_{av}/k_{NO}} = \gamma \left(\frac{[NO_x]_o}{j_{av}/k_{NO}}\right)^a \exp\left\{-\frac{E_{0H}}{kT}\right\}^b \times f(R;\beta_{av},\alpha_1,\alpha_2,\lambda) \tag{12}$$

and $\beta_{av} = \beta' J^{-c}$

$\gamma = 3.45\times10^5, \lambda = 0.62, \alpha_1 = 2.5, \alpha_2 = 0.69$

$a = 0.65, b = 6.1$

$\beta' = 413, c = -0.81$

This "universal" curve captures the variability of maximum ozone concentration over a wide range of NO_x and OLT concentrations, as well as a range of actinic fluxes and temperatures typical of ozone formation in urban environments (National Research Council, 1991). A total of 8 parameters are needed to fully characterize this variability. It must be pointed out Eq. (12) (or any other suitable parameterization for the similarity relationship) is merely a means of quantifying the similarity relationship and should not be confused with scaling itself, who's success is independent of this parameterization.

5 Discussion

While, the universal similarity relationship arises because the integrated behaviour of the VOC to NO_x ratio, temperature and the level of actinic flux on maximum ozone concentration can be captured by a power law relationship involving a small number non-dimensional quantities, none of the parameters appears to be directly related to any rate constants or reaction products in the chemical mechanisms studied. Instead, these scaling parameters appear to be related to subprocesses within the photochemical system. For instance, the dependence of the similarity relationship on R suggests that once maximum ozone concentrations have been normalized by initial NO_x concentrations (which itself is proportional to the highest ozone concentrations that can be achieved for a given initial NO_x concentration; independent of VOC concentration, Blanchard et al., 1999), the photochemical system's behaviour with respect to this scaled ozone concentration depends only on the relative abundance of VOC to NO_x. From a radical propagation perspective (Tonnesen and Dennis, 2000), R acts as a surrogate for the dependence ozone production shows to the fraction of $OH^\bullet$ radicals reacting with VOCs and the fraction of $HO_2^\bullet$ radicals that react with NO; the first of which increases with higher VOC levels, the second to higher NO_x levels. The dependence of the scaling break (β) on actinic flux (J) suggests increasing J causes the switch in regimes to occur for lower R-values but otherwise leaves the integrated behaviour of the photochemical system unchanged. The power law dependence on $\overline{T}$ suggests the integrated effects of temperature on ozone affects only the magnitude of the final concentrations while leaving the R and J dependencies unchanged (this is an approximation, since temperature also affects the scaling break, with increasing temperatures causing the break to occur at smaller R-values, Ainslie, 2004).

The set of dependent dimensionless groups used to parameterize the behaviour of the various photochemical mechanisms can be compared with findings from a local sensitivity analysis of the RADM2 mechanism (Gao et al., 1995). While the aims of that analysis differs from ours (identification of specific reaction and photolysis rate constants whose uncertainty lead to the largest uncertainty in modeled ozone concentrations versus representing the integrated behaviour of RADM2 by as few variables as possible), they show several common traits. First, the sensitivity analysis shows ozone is relatively insensitive to the parameters of about 90% of the reactions in RADM2, consistent with our scaling of integrated model behaviour using only a few variables. Secondly, their analysis shows ozone sensitivities are strongly dependent on the VOC to NO_x ratio, consistent with the central role played by R in the scaling. Next, they show the strong dependence of ozone on the NO_2, HCHO and O_3 photolysis reactions. In the present analysis, J acts as a surrogate for the total actinic flux and we assume that changes in J can account for all changes in photolytic activity along the various photolytic pathways. Finally, Gao et al. (1995) show modeled ozone concentrations are more sensitive to the NO_2 + OH reaction than most of the VOC the $OH^\bullet$ reactions. This suggests that NO_2+OH might have been a better reaction for the OH-pathway reactions than the VOC+OH reaction used here. However, Tonnesen (1999) shows peak ozone concentrations in RADM2 box model simulations are not strongly affected by changes in k_{HNO3} because of strong feedback loops which buffer peak ozone concentrations from changes in the mechanism. Thus the choice of variables used to account for the radical reaction pathways may have little impact on the scaling. It is the integrated behaviour of these feedback loops, and their sensitivity to the relative abundance of VOC to NO_x, that the scaling analysis captures. While each chemical mechanism accounts for these feedback loops by different means, the similarity relationships show these loops express themselves in a common manner.

The most striking feature of the scaling analysis is the scaling break which is readily apparent for most VOC and VOC mixtures. The easiest way of relating the scaling break to the underlying chemistry is through a sensitivity analysis using a chemical mechanisms. Such analyses show the scaling break is not uniquely related to any single parameter in the mechanisms studied so far (Ainslie, 2004). Instead, it sensitive to changes in many rate constants and reaction products, with changes that affect β often affecting the other parameters. Equation 10 shows that it is the shape parameter (α) that changes across the break. For the RADM2 mechanism, α_1 shows more variability between VOC classes than does α_2 (which is largely independent of VOC class). In a simple autocatalytic description of ozone formation, ozone production is initially slow because it is limited by radical availability. But as ozone concentrations begin to rise, ozone acts as a radical source, increasing its own production rate. This positive feedback leads to conditions with elevated NO_2 and $OH^\bullet$ concentration which spurs on HNO_3 formation, limiting ozone production. From another point of view, when additional NO_x is added to a VOC-NO_x mixture, ozone concentrations decrease because: initially, there is more NO that has to be oxidized to NO_2; this greater amount of NO to oxidize causes ozone formation to occur later, delaying the inorganic production of radicals; and finally, increased NO_2 concentrations decrease the propagation efficiency of $OH^\bullet$ and favour the production of HNO_3 (Tonnesen and Jeffries, 1994). As a result, VOCs that can produce their own photolytic radical source can alleviate this dependence of ozone production on ozone concentration – that is, they should show less NOx-inhibition. From the perspective of the scaling model, we find the RADM2 HCHO class, which readily produces radicals through photolysis, has the lowest α_1 value (1.5) while TOLU, with the highest value (3.1), does not photolyze nor does it produce many carbonyl compounds as OH-reaction products. Furthermore, it is possible to show α_1 is directly associated with the tilting of ozone isopleths above the ridgeline (Ainslie, 2004), which can be viewed as

a geometric representation of NOx-inhibition. On the other side of the break, ozone formation appears to be less dependent on VOC species, which might be expected under NOx-sensitive conditions. The scaling break is also found to be closely associated with a fixed value of the fraction of $HO_2^\bullet$ radicals that react with NO (f_{HO2+NO}); and less closely associated with both the maximum in OH-chain length that occurs above the ridgeline and the peak in $OH^\bullet$ production also seen above the ridgeline (Ainslie, 2004).

The scaling methods have also been applied to smog chamber data (Ainslie, 2004) where the methods allow observations from a variety of experiments, having different initial precursor concentrations, temperatures and actinic fluxes, to be presented on a single graph. Only a slight break in the corresponding Weibull transformed observations is observed with the chamber data and the analysis cannot tell if the lack of sharp break is due to experimental uncertainties stemming from the presence of the chamber membrane (especially if this acts as additional radical source, reducing the NO_x-inhibition of the chamber VOC mixture); a bias in test conditions with more experiments performed at R-values below the scaling break; or if chemical mechanisms overly enhance the process leading to the scaling break. More research is needed in this area, perhaps making use of ambient ozone concentrations drawn from a variety of environments.

6 Conclusions

Eulerian photochemical models are the principle means used to study tropospheric ozone at urban, regional and continental scales. Central to these models are their photochemical mechanisms. In this paper, we have used dimensional analysis, commonly used in many branches of atmospheric science, to provide simple representations of the behaviour of several photochemical mechanisms. Our research shows dimensionless maximum ozone concentration ($\overline{[O_3]}$) can be described by a product of powers of dimensionless initial NO_x concentration ($\overline{[NOx]}$), dimensionless temperature ($\overline{T}$) and a similarity curve (f) directly dependent on the ratio of initial VOC to NO_x concentration (R) and internally dependent on the cumulative NO_2 photolysis rate (J). The scaled dimensionless model output, when Weibull transformed, exhibits a striking scaling break which suggests the photochemical system switches governing regimes. The break coincides closely (but not exactly) with a change in ozone sensitivity to initial NO_x concentration (the ridgeline on an isopleth diagram). This close but not exact relationship is also seen between the scaling break and maxima in $OH^\bullet$-production and $OH^\bullet$-chainlength (Ainslie, 2004). The regime switch, revealed here through a scaling analysis using model output, can be compared with similar findings using different approaches: Johnson's (1984) parameterization of ozone formation into light- and NO_x-limited regimes based on smog chamber data; the Kleinman (2005) radical budget analysis of ozone production ($d[O_3]/dt$) sensitivities to [VOC] and [NO] based on a simplified photochemical reaction set; and the Sillman (1995) analysis of a simplified set of reactions to identify NO_x- and VOC-sensitive regions using observed concentrations of certain long-lived "indicator" species.

A parameterization for the similarity relationship has been developed which captures the complex dependence of ozone formation over a wide range of initial precursor concentrations: above, below and around the ridgeline. This represents an improvement over similar efforts by Johnson (1984) and Chang and Rudy (1993). The similarity function predicts, in the NO_x-limited region, maximum ozone concentration to be a function of initial NO_x concentration only, consistent with Chang and Suzio (1995), Blanchard et al. (1999) and Johnson (1984). The similarity function has six parameters (a, γ, β, λ, α_1 and α_2) and in general, all six vary between VOC classes with γ and β showing the greatest variability while a and α_2 the least. Two more parameters are needed to include the influence of actinic flux and temperature on the similarity relationship. We find the qualitative features of the similarity relationship hold for a wide range of VOCs, VOC mixtures and for other chemical mechanisms and plotting Weibull transformed dimensionless model output as a function of $\ln R$ provides a new way of representing the behaviour of a photochemical mechanism. The scaling methods have allowed us to include temperature and actinic flux dependencies in the development of a "universal" similarity function. While the sum of ozone produced and NO oxidized provides a more complete description of the photochemical oxidation process, we find the scaling analysis and similarity function are qualitatively the same when using oxidized NO + O_3 produced instead of O_3. Finally, while running a box model with a chemical mechanism is fast and accurate way to calculate ozone concentrations, the use of Eqs. (10) or (12) to estimate ozone concentrations offer the potential to include photochemistry in bigger integrated assessment models where computation resources are limited.

While our analysis suggests that over a wide range of initial precursor concentrations and environmental conditions, and when viewed from the proper perspective (provided by the scaling analysis), the complex behaviour of a photochemical mechanism can be simply described, it must be stressed that this high-level representation is not intended to accurately describe the internal workings of a photochemical system but rather to accurately reproduce the behaviour of a chemical mechanism (whether or not chemical mechanisms faithfully represent actual ozone formation is a difficult but different question). Furthermore, in order to facilitate the analysis of our results, we have studied photochemical mechanisms in isolation from important physical processes like deposition and entrainment. An investigation of how these physical processes compete with chemical processes could be achieved by a scaling-level analysis of model output from idealized 3-D Eulerian simulations.

Acknowledgements. Funding for this research was through the University of British Columbia graduate fellowships (UGF), the National Science and Engineering Research Council (NSERC) and the Canadian Foundation for Climate and Atmospheric Sciences (CFCAS). Special thanks to A. Rickard at the University of Leeds for the MCM simulations.

Edited by: A. Volz-Thomas

References

Ainslie, B. D.: A Photochemical Model Based on a Scaling Analysis of Ozone Photochemistry, Ph.D. thesis, University of British Columbia, Vancouver, B.C., Canada, 311 pp., 2004.

Atkinson, R.: Atmospheric chemistry of VOCs and NOx, Atmos. Environ., 34, 2063–2101, 2000.

Azzi, M., Johnson, G. M., and Cope, M.: An introduction to the Generic Reaction Set, in: Proceedings of the 11th international Clean Air Conference, Brisbane Australia, 1992.

Barenblatt, G. I.: Scaling, Self-similarity, and Intermediate Asymptotics, Cambridge University Press, Cambridge, UK, 386 pp., 1996.

Birkhoff, G.: Hydrodynamics, Princeton University Press, Princeton, NJ, 184 pp., 1950.

Blanchard, C. L., Lurman, F. W., Roth, P. M., Jeffries, H. E., and Korc, M.: The use of ambient data to corroborate analyses of ozone control strategies, Atmos. Environ., 33, 369–381, 1999.

Bridgman, P. W.: Dimensional Analysis, Yale University Press, New Haven, CT., USA, 113 pp., 1937.

Carter, W. P. L.: A detailed mechanism for the gas-phase atmospheric reactions of organic compounds, Atmos. Environ., 24A, 481–518, 1990.

Chang, T. Y. and Rudy, S. J.: Ozone-precursor relationships: a modeling study of semi-empirical relationships, Environ. Sci. Technol., 27, 2213–2219, 1993.

Chang, T. Y. and Suzio, M. J.: Assessing ozone-precursor relationships based on a smog production model and ambient data, J. Air Waste Manage. Assoc., 45, 20–28, 1995.

Dodge, M. C.: Chemical oxidant mechanisms for air quality modeling: critical review, Atmos. Environ., 34, 2103–2130, 2000.

Gao, D., Stockwell, W. R., and Miford, J. B.: First-order sensitivity and uncertainty analysis for a regional-scale gas-phase chemical mechanism, J. Geophys. Res., 100, 23 153–23 166, 1995.

Gery, M. W., Whitten, G. Z., Killus, J. P., and Dodge, M. C.: A photochemical kinetics mechanism for urban and regional scaled computer modeling, J. Geophys. Res., 94, 12 925–12 956, 1989.

Haagen-Smit, A. J.: Chemistry and physiology of Los Angeles smog, Ind. Eng. Chem., 44, 1342–1346, 1952.

Jeffries, H. E. and Tonnesen, S.: A Comparison of two photochemical reaction mechanisms using mass balance and process analysis, Atmos. Environ., 28, 2991–3003, 1994.

Jeffries, H. E., Sexton, K. G., Arnold, J. R., and Kale, T. L.: Validation testing of New Mechanisms with outdoor Chamber data. Volume 2: Analysis of VOC Data for the CB4 and CAL photochemical mechanisms., Tech. Rep. EPA-600/3-89-010b, U.S. Environmental Protection Agency, 1986.

Johnson, G. M.: A simple model for predicting ozone concentration of ambient air, in: Proceedings of the Eighth International Clean Air Conference, pp. 716–731, Melbourne Australia, 1984.

Kleinman, L. I.: The dependence of tropospheric ozone production rate on ozone precursors, Atmos. Environ., 39, 575–586, 2005.

Lonneman, W. A.: Comparison of 0600-0900 AM Hydrocarbon Compositions Obtained from 29 Cities, in: Proceedings of the 1986 EPA/APCA Symposium on Measurement of Toxic Air Pollutants, 419 pp., 1986.

National Research Council: Rethinking the Ozone Problem in Urban and Regional Air Pollution, National Academy Press, Washington, D.C., 500 pp., 1991.

Pryor, S. C. and Steyn, D. G.: Hebdomadal and Diurnal cycles in ozone time series from the Lower Fraser Valley, B. C., Atmos. Environ., 29, 1007–1019, 1995.

Saunders, S. M., Jenkin, M. E., Derwent, R. G., and Pilling, M. J.: Report Summary: World Wide Web site of a master chemical mechanism (MCM) for use in tropospheric chemistry models, Atmos. Environ., 31, 1249, 1997.

Shenvi, N., Geremia, J. M., and Rabitz, H.: Efficient chemical kinetic modeling through neural network maps, J. Chem. Phys., 120, 9942–9951, 2004.

Sillman, S.: The use of NO_y, H_2O_2 and HNO_3 as indicators for ozone-NOx-hydrocarbon sensitivity in urban locations, J. Geophys. Res., 100, 14 175–14 188, 1995.

Stockwell, W. R., Middleton, Chang, J., and Tang, X.: The second generation regional acid deposition model chemical mechanism for regional air quality modeling, J. Geophys. Res., 95, 16 343–16 367, 1990.

Stockwell, W. R., Kirchner, F., and Kuhn, M.: A new mechanism for regional atmospheric chemistry modeling, J. Geophys. Res., 102, 25 847–25 879, 1997.

Stull, R. B.: An Introduction to Boundary Layer Meteorology, Kluwer Academic Publishers, Dordrecht, The Netherlands, 670 pp., 1988.

Taylor, G. I.: The formation of a blast wave by a very intense explosion. II. The atomic explosion of 1945, Proc. Roy. Soc., A201, 175–186, 1950.

Tonnesen, G. S.: Effects of uncertainty in the reaction of the hydroxyl radical with nitrogen dioxide on model-simulated ozone control strategies, Atmos. Environ., 33, 1587–1598, 1999.

Tonnesen, G. S.: User's Guide for OZIPR Version 2.0, Tech. rep., National Research and Exposure Assessment Laboratory, U.S. EPA, Research Triangle Park, North Carolina, USA, 2000.

Tonnesen, G. S. and Dennis, R. L.: Analysis of radical propagation efficiency to assess ozone sensitivity to hydrocarbons and NOx 1. Local indicators of instantaneous odd oxygen production sensitivity, J. Geophys. Res., 105, 9213–9225, 2000.

Tonnesen, S. and Jeffries, H. E.: Inhibition of odd oxygen production in the Carbon Four and Generic Reaction Set mechanism, Atmos. Environ., 28, 1339–1349, 1994.

Wang, S. W., Georgopoulos, P. G., Li, G., and Rabitz, H.: Computationally Efficient Atmospheric Chemical Kinetic Modeling by means of high dimensional model representation HDMR, Lecture Notes in Computer Science, 2179, 326–333, 2001.

West, G. W., Brown, J. H., and Enquist, B. J.: A General model for the origin of biometric scaling laws in biology, Science, 276, 122–126, 1997.